

Experimental study on flame pattern formation and combustion completeness in a radial microchannel

Aiwu Fan^{1,2}, Sergey Minaev³, Sudarshan Kumar⁴, Wei Liu² and Kaoru Maruta¹

¹ Institute of Fluid Science, Tohoku University, 2-1-1 Katahira, Aoba-ku, Sendai 980-8577, Japan

² School of Energy and Power Engineering, Huazhong University of Science and Technology, Wuhan 430074, People's Republic of China

³ Institute of Theoretical and Applied Mechanics, SB-RAS Novosibirsk 630090, Russia

⁴ Aerospace Engineering Department, IIT Bombay, Powai, Mumbai 400076, India

E-mail: faw@edyn.ifs.tohoku.ac.jp

Received 1 August 2007, in final form 19 September 2007

Published 25 October 2007

Online at stacks.iop.org/JMM/17/2398

Abstract

Combustion behavior in a radial microchannel with a gap of 2.0 mm and a diameter of 50 mm was experimentally investigated. In order to simulate the heat recirculation, which is an essential strategy in microscale combustion devices, positive temperature gradients along the radial flow direction were given to the microchannel by an external heat source. A methane–air mixture was supplied from the center of the top plate through a 4.0 mm diameter delivery tube. A variety of flame patterns, including a stable circular flame and several unstable flame patterns termed unstable circular flame, single and double pelton-like flames, traveling flame and triple flame, were observed in the experiments. The regime diagram of all these flame patterns is presented in this paper. Some characteristics of the various flame patterns, such as the radii of stable and unstable circular flames, major combustion products and combustion efficiencies of all these flame patterns, were also investigated. Furthermore, the effect of the heat recirculation on combustion stability was studied by changing the wall temperature levels.

(Some figures in this article are in colour only in the electronic version)

Nomenclature

ϕ	Equivalence ratio
\varnothing	Diameter
η	Combustion efficiency
r	Radial location in the microchannel
T_{bottom}	Wall temperature at the inner surface of the bottom plate
T_{top}	Wall temperature at the inner surface of the top plate
V_{in}	Inlet velocity at the delivery tube

1. Introduction

With advances in modern science and technology, a variety of compact devices, such as cellular phones, notebook computers, portable electronics, microrobots, microaerial vehicles and so on, have come into use in the past few decades. Most of these small systems are currently powered by electrochemical batteries which have disadvantages of a short life span, long recharging periods and low energy densities. To overcome these disadvantages, combustion-based power-generating devices have been recognized as one of the most promising choices due to 20–50 times

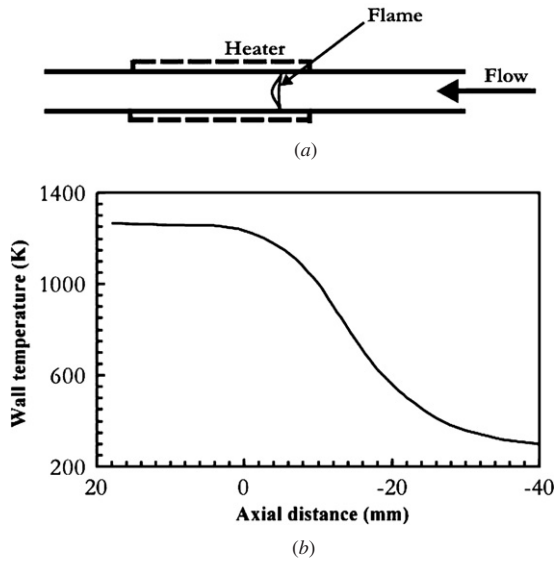


Figure 1. Combustion in a 2 mm diameter 1D straight tube with heat recirculation: (a) schematic of the straight tube, (b) wall temperature profile. The axial distance of zero indicates the beginning location of the heater [17].

higher energy densities of hydrocarbon fuels as compared with those of electrochemical batteries [1, 2]. These miniaturized combustion-based power sources also show other merits, including lower pollutant emissions, especially NO_x , due to the lower operating temperature of these systems as compared with those of conventional systems [1, 3]. Micro-combustors can be used as efficient heaters for steam reformers in integrated micromechanical systems to produce hydrogen for small-scale fuel cell applications [4]. It is also a key component of the micro gas turbine engine and microthermophotovoltaic systems, which have been extensively studied in recent years [5–13]. However, the increased heat loss due to a large surface area-to-volume ratio adversely affects the combustion stability limits in devices and systems employing microscale combustion. For stable combustion, thermal management, for instance heat recirculation, is a key factor for efficient operation of these microscale combustion devices [3, 14]. In this technique, the temperature of combustor walls in the downstream region remains high due to the heat of combustion, and the incoming mixture is preheated by the walls through heat recirculation. Many studies [15, 16] have demonstrated that thickness and thermal properties of the solid walls play an important role in the heat recirculation performance of the system configuration.

Recently, Maruta *et al* [17] studied the combustion behavior in a microchannel. They used a straight quartz tube with a positive temperature gradient along the flow direction to simulate a 1D microchannel with heat recirculation, as is shown in figure 1. In their investigation, both stable and unstable flames were observed. Based on this work [17], Kumar *et al* [18–20] extended it to the 2D case, as is shown in figure 2. A radial microchannel with a positive temperature gradient along the radial flow direction was utilized in their work to simulate a 2D microchannel with heat recirculation, which is somewhat like the combustor of the MIT gas turbine

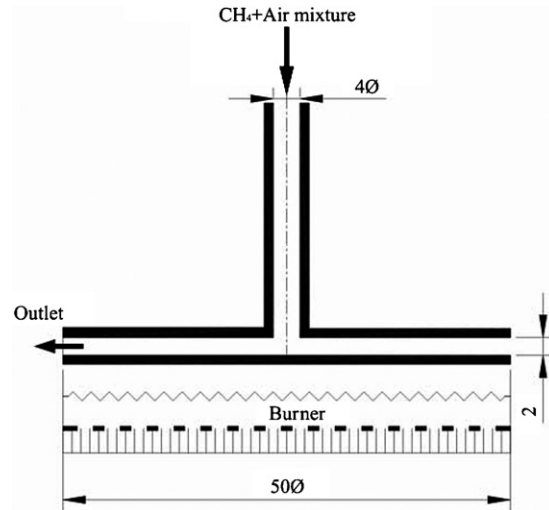


Figure 2. Schematic diagram of the experimental setup.

engine [5–7]. Such a configuration enables a visualization study on flame behavior in the radial microchannel. In addition to a normal stable circular flame, various unstable flame patterns, such as traveling flame, pelton-like flame, triple flame [19] (note that the term ‘triple flame’ in the present paper is used to indicate a flame pattern with three branches; it is different from the conventional definition of a ‘triple flame’ known by the combustion community.), etc. were observed. However, their studies were mainly focused on the combustion characteristics at equivalence ratios of 0.67 and 0.85, and thus the current knowledge of combustion behavior in this microchannel is limited. Hence, in the present work, systematic experiments were carried out over an equivalence ratio range from 0.65 to 1.30, to investigate the combustion behavior in a radial microchannel with a gap of 2.0 mm, which was identical to that used by Kumar *et al* [18–20]. Herein reported is the regime diagram of those flame patterns, as well as radius variation tendencies of circular flames, combustion emissions and combustion efficiencies of all the stable and unstable flame patterns. Meanwhile, the effect of the heat recirculation on the combustion stability is also experimentally investigated in this work. Based on these experimental results, recommendations were made to facilitate an efficient design and operation of such kind of geometry for micro-combustor applications. The present paper focuses on the flame pattern formations and their effects on the combustion completeness and efficiency in this radial microchannel.

2. Experimental setup and wall temperature profiles

A schematic diagram of the experimental setup is shown in figure 2. Two circular quartz plates ($\varnothing 50$) were maintained parallel to each other within an accuracy of $\pm 0.1^\circ$, with the help of a level indicator. The flatness of quartz plates was 0.01 mm per mm. To simulate heat recirculation through channel walls, wall temperature profiles were created with a porous burner. This approach is equivalent to thermally thick walls, which were also employed in the series of previous studies [17–21]. A methane–air mixture was injected at the center of the top plate through a delivery tube with a

diameter of 4.0 mm. Wall temperatures of the microchannel were measured with a 300- μm -sized *K*-type thermocouple. The measured temperatures were corrected for heat loss from the thermocouple bead, and the corrected temperatures are accurate to ± 5 K of the actual value. The mixture delivery tube was designed to maintain the upstream temperature of the incoming mixture at 300 K. The flow rate of the supplied methane–air mixture was monitored through electric mass flow controllers within an accuracy of $\pm 1\%$. In order to maintain a laminar flow in the delivery tube, the maximum value of mixture velocity at the delivery tube was set at 7.0 m s^{-1} , where the representative Reynolds number is ~ 1800 [18–20]. Methane gas of 99.99% purity was used as fuel during the present investigations. The flame visualization studies were carried out with a still digital camera. The uncertainties in the measured flame radius are expected to remain less than 5% of the measured values. Movie recordings of various flame patterns were carried out with an image-intensified high-speed video camera right after the mixture was ignited in the microchannel. Captured images were analyzed using the software PFV-Ver.2.4.2.0. Exhaust gas analysis was carried out with a ‘Shimadzu GC-14B’ gas chromatograph. A sample of $500 \mu\text{l}$ was drawn with a microsyringe and fed into the gas analyzer. Mole fractions of the major species, such as CO_2 , CO , CH_4 and O_2 , were determined. The uncertainties in the measurements of exhaust gas emissions are less than 3% of the measured values.

Each time before the methane–air mixture was introduced into the microchannel, wall temperatures were required to be a steady state by airflow at the same inlet velocity as that of the fuel–air mixture. Figure 3 shows the typical wall temperature profiles at an inlet airflow velocity of 4.0 m s^{-1} . The microchannel was heated by a porous metal burner at a constant air flow rate and a constant propane gas flow rate unless otherwise stated. Both radiation and convection modes play significant roles in the heat transfer processes between the top and bottom plates. Meanwhile, heat conduction in the solid walls is also very important. From figure 3, it can be seen that temperature profiles at the inner surfaces of the bottom and top walls were similar. Also noted is that the inner surface temperature of the bottom wall was ~ 30 – 50 K higher than that of the top wall at locations of a large radius, while in small radius regions the inner surface temperature of the bottom wall was ~ 30 – 50 K lower than that of the top wall because of the downward cold jet flow from the delivery tube.

3. Experimental results and discussion

3.1. Flame patterns and regime diagram

A variety of flame patterns, including a stable circular flame and five kinds of unstable flame patterns [18–20], termed unstable circular flame, traveling flame, single and double pelton-like flames and triple flame, are observed in the present study. Photos taken with an image-intensified high-speed camera of these flame patterns are presented in figure 4. The regime diagram of all these flame patterns is shown in figure 5, in which the nodes without symbols mean that no flame was observed under these conditions. In this regime diagram,

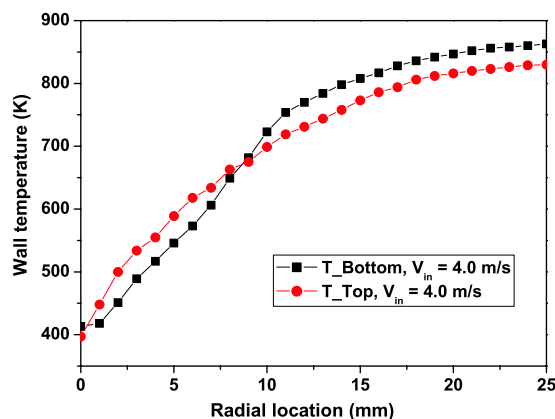


Figure 3. Measured temperature profiles of the bottom and top plates when $V_{in} = 4.0 \text{ m s}^{-1}$. The microchannel was heated from the bottom with a porous metal burner at a constant air flow rate and a constant propane gas flow rate.

increment steps of equivalence ratio and inlet mixture velocity are 0.05 and 0.5 m s^{-1} , respectively. For the convenience of discussion, the inlet mixture velocity at the delivery tube is used as the horizontal axis instead of the mixture flow rate for all the figures in this paper.

From figure 5, it is noted that most of the regime diagram is occupied by the stable circular flame pattern, which demonstrates that the methane–air mixture can achieve a stable combustion in this microchannel under these conditions. As is shown in figure 4(a), the flame front of this pattern is a stable, symmetric circle with uniform luminosity. The radial location of the stable circular flame front is a function of the inlet mixture velocity and mixture equivalence ratio, which will be discussed in detail in section 3.2. When the inlet mixture velocity was 1.5 m s^{-1} , the flame was stabilized at the inlet port of the radial microchannel.

For very lean and rich mixtures, single and double pelton-like flames were observed, as is shown in figures 4(c) and (d) respectively. These two kinds of pelton-like flames rotate around the center of the configuration at a frequency of approximately 24–58 Hz. Moreover, it was found that the double pelton-like flame only appeared in the inlet mixture velocity ranges of 3.5 – 5.0 m s^{-1} for $\phi = 0.65$ and 4.0 – 5.5 m s^{-1} for $\phi = 1.30$ at a random possibility. In the region between those occupied by the pelton-like flames and the stable circular flame, the traveling flame pattern was observed. With visual observation, the traveling flame looks like a closed circle with non-uniform luminosities. With further observation with an image-intensified high-speed camera, it can be seen that a flamelet, which is geometrically similar to the single pelton-like flame, emanates from one end of the luminous flame and then travels toward the opposite end. At the moment of its approach, the opposite end of the luminous flame also generates a pelton-like flamelet which merges with the approaching one. This merger can be clearly seen in figure 4(e). Another major characteristic of the traveling flame is the relatively loud noise produced by the combustion process. We suppose that it is produced at the moment when those two pelton-like flamelets merge with each other in opposite rotating directions.

When the inlet mixture velocity was increased to 6.5 and 7.0 m s^{-1} , the flame front of the circular flame became unstable

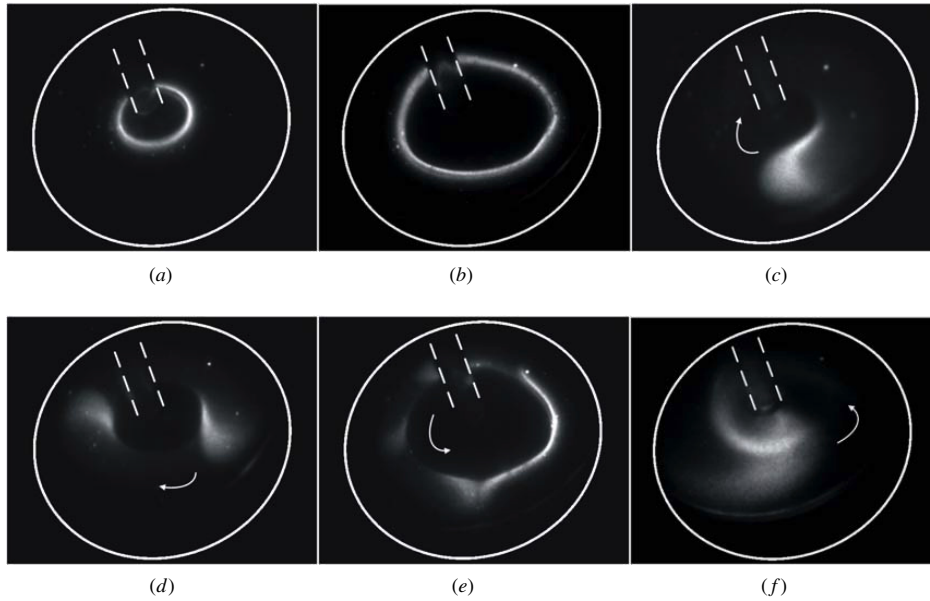


Figure 4. One shot photos of different flame patterns taken with an image-intensified high-speed video camera at a rate of 500 frames per second with a shutter speed of $1/500$ s from a top-side viewpoint: (a) stable circular flame, (b) unstable circular flame, (c) single pelton-like flame, (d) double pelton-like flame, (e) traveling flame and (f) triple flame. The solid and dashed white lines indicate the positions of the top plate and mixture delivery tube, respectively. The arrows are drawn to indicate the rotating direction of the rotating flame patterns.

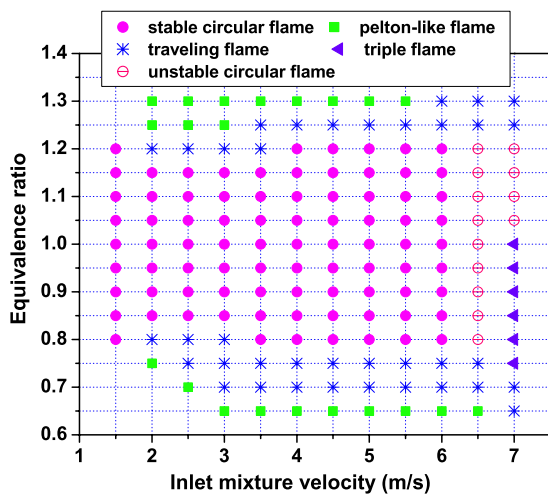


Figure 5. Regime diagram of flame patterns. The microchannel was heated from the bottom with a porous metal burner at a constant airflow rate and a constant propane gas flow rate.

(see figure 4(b)). Although the flame front was still closed and being an entire circle, it deformed spatio-temporally. Different locations of the flame front had different radii and curvatures. At an inlet mixture velocity of 7.0 m s^{-1} and over the equivalence ratio range of $0.75\text{--}1.0$, the triple flame appeared, as is shown in figure 4(f). It is interesting to note that transitions from a triple flame to an unstable circular flame and vice versa were sometimes observed, which demonstrates the highly unstable nature of flames under those conditions.

3.2. Radius variation of the circular flame

The radial location of the circular flame depends on the balance between the local flame propagation velocity and the flow velocity of the fuel–air mixture. The circular flame radius is

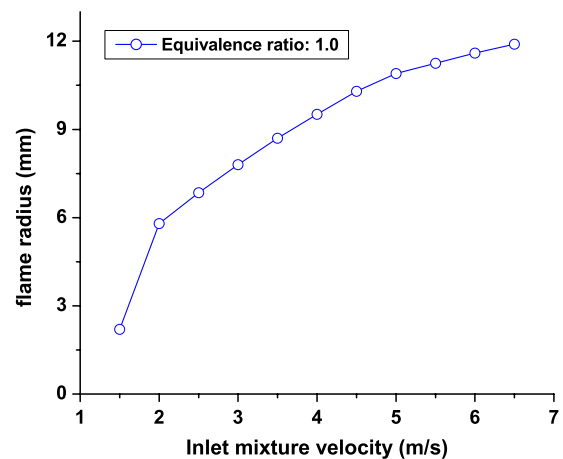


Figure 6. Radius variation of circular flames versus inlet mixture velocity when $\phi = 1.0$.

a function of both the inlet mixture velocity and the mixture equivalence ratio, as shown in figures 6 and 7 respectively. From figure 6, it can be seen that when $V_{\text{in}} = 1.5 \text{ m s}^{-1}$, the flame radius was $\sim 2.0 \text{ mm}$ as the flame was stabilized at the inlet port of the microchannel. Then, the radius of the stable circular flame increased nearly linearly as the inlet mixture velocity was varied from 2.0 m s^{-1} to 5.0 m s^{-1} . In the high inlet mixture velocity region of $5.5\text{--}6.5 \text{ m s}^{-1}$, the increase in the flame radius slowed down (note that the radius of the unstable circular flame at $V_{\text{in}} = 6.5 \text{ m s}^{-1}$ was the mean value of eight different angular locations of the flame front). It is noted from figure 6 that the flame radius at $V_{\text{in}} = 6.0 \text{ m s}^{-1}$ was about six times that at $V_{\text{in}} = 1.5 \text{ m s}^{-1}$. From figure 7, it can be seen that at a constant inlet mixture velocity of 4.0 m s^{-1} , the flame radius exhibited its minimum at stoichiometry which can be reasonably explained by the laminar burning velocity dependence on the mixture equivalence ratio. Taken as a

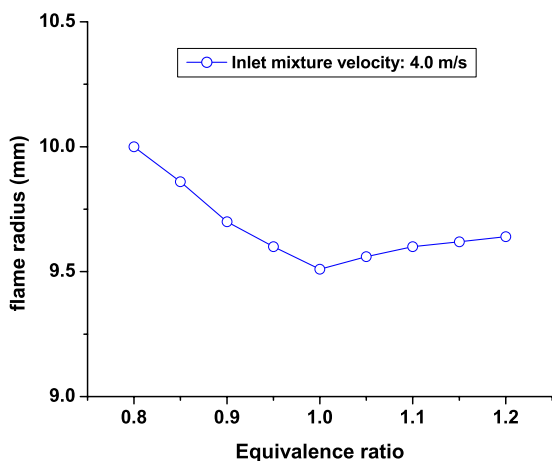


Figure 7. Radius variation of the stable circular flame versus mixture equivalence ratio when $V_{in} = 4.0 \text{ m s}^{-1}$.

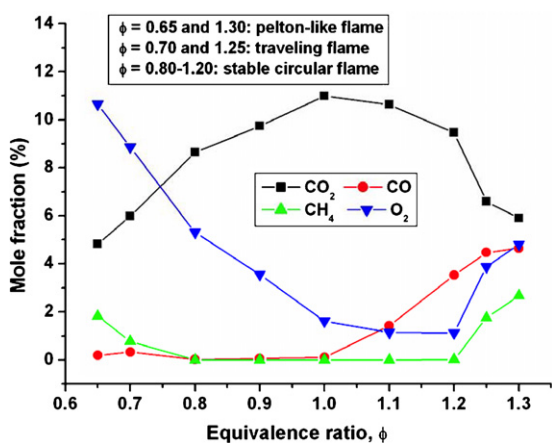


Figure 8. Mole fractions of CO_2 , CH_4 , CO and O_2 in the exhaust gas versus mixture equivalence ratio when $V_{in} = 4.0 \text{ m s}^{-1}$.

whole, radius variation with the mixture equivalence ratio of the stable circular flame was relatively small.

3.3. Exhaust gas analysis and combustion efficiency

The emission characteristics of this radial microchannel were measured for all the stable and unstable flame patterns. Combustion efficiency (or chemical conversion efficiency) was calculated based on the exhaust gas analysis to examine the overall incompleteness of the combustion process. It is defined as [9]

$$\eta = \frac{\text{total enthalpy released}}{\text{possible maximum enthalpy release}}$$

Here, the total enthalpy released is that the possible maximum enthalpy release of CH_4 in the fresh mixture subtracts the unreleased enthalpies of CH_4 and CO in the exhaust gas.

Figures 8 and 9 respectively show the variations of major combustion product concentrations and combustion efficiency with the mixture equivalence ratio at $V_{in} = 4.0 \text{ m s}^{-1}$. From figure 8, it can be seen that in the equivalence ratio range of 0.8–1.2 (corresponding to stable circular flames), no unburned CH_4 was detected in the exhaust gas. However, although the

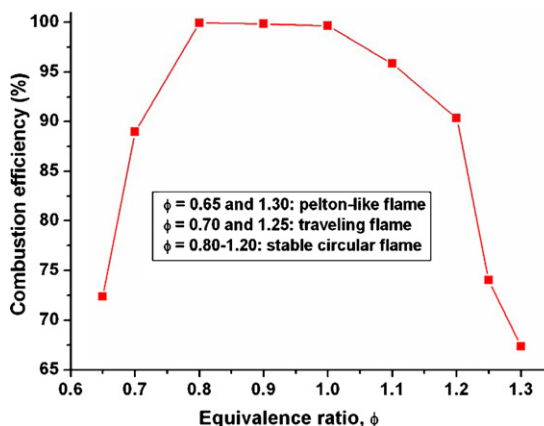


Figure 9. Combustion efficiency versus mixture equivalence ratio when $V_{in} = 4.0 \text{ m s}^{-1}$.

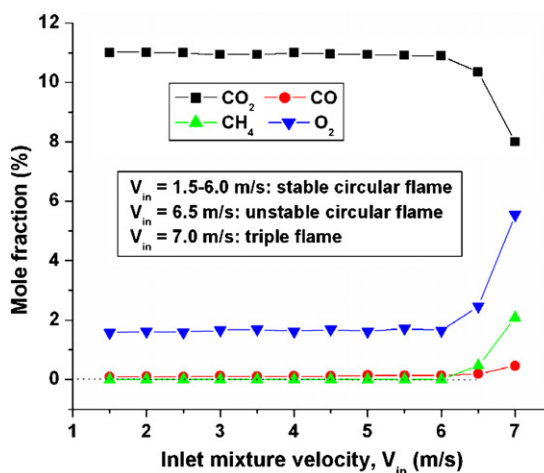


Figure 10. Mole fractions of CO_2 , CH_4 , CO and O_2 in the exhaust gas versus inlet mixture velocity when $\phi = 1.0$.

CO concentration was very low for the stable circular flame when $\phi = 0.8\text{--}1.0$, it increased drastically for the cases of $\phi = 1.1\text{--}1.2$. As a result, when the equivalence ratio increased from 0.8 to 1.2, the combustion efficiencies decreased from $\sim 99.9\%$ to $\sim 90.4\%$. Variation tendencies of combustion products for the stable circular flames in our experiments were confirmed to be similar to those of the adiabatic flames based on chemical equilibrium calculations. This demonstrates that nearly complete combustion occurred in the stable circular flame in the radial microchannel. For the cases of $\phi = 0.70$ and 1.25, which correspond to traveling flames, large amount of CH_4 and CO emissions were detected in the exhaust gas (note that in these cases, the samples were made from the traveling part of the flame front) and the combustion efficiencies were $\sim 89.0\%$ and $\sim 74.0\%$, respectively (see figure 9). When $\phi = 0.65$ and 1.30, which correspond to the pelton-like flames (note that here the samples of the combustion products were made from the single pelton-like flames), the CH_4 concentrations in the exhaust gases were even larger than those of $\phi = 0.70$ and 1.25. However, the CO concentrations of $\phi = 0.65$ and 1.25 were less than those of $\phi = 0.70$ and 1.30, respectively. This demonstrates that the CO concentration in the exhaust gas exhibited a positive correlation with the mixture equivalence

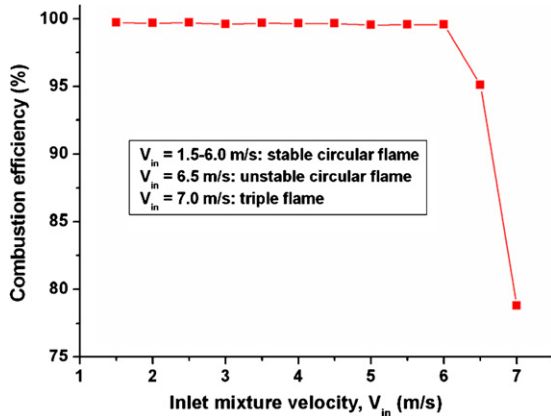


Figure 11. Combustion efficiency versus inlet mixture velocity when $\phi = 1.0$.

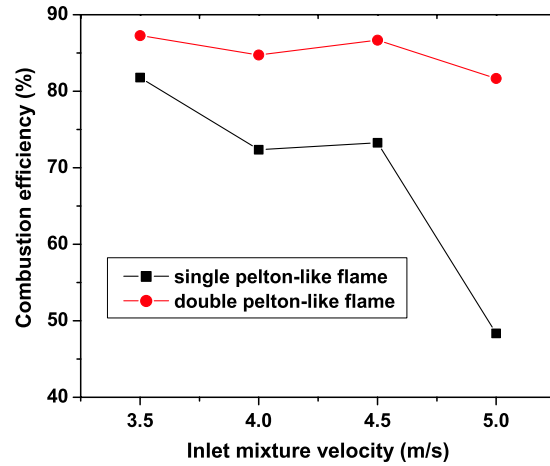


Figure 13. Combustion efficiency versus inlet mixture velocity for single and double pelton-like flames when $\phi = 0.65$.

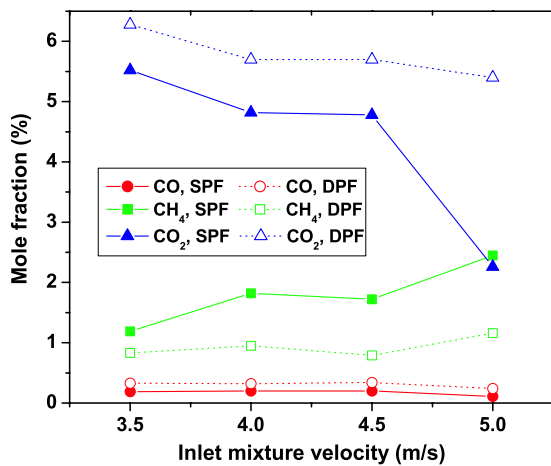


Figure 12. Mole fractions of CO₂, CH₄ and CO in the exhaust gas versus inlet mixture velocity for single and double pelton-like flames when $\phi = 0.65$. SPF and DPF represent single and double pelton-like flames, respectively.

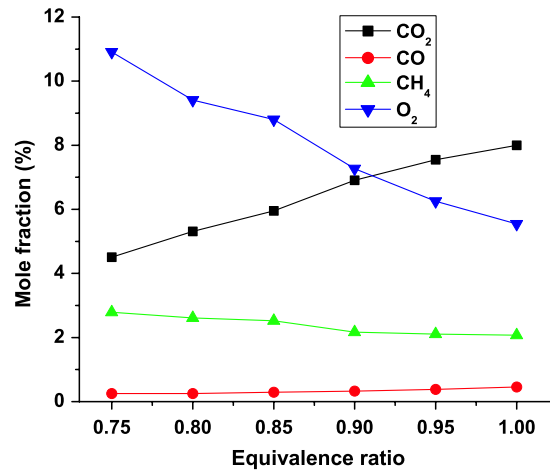


Figure 14. Mole fractions of CO₂, CH₄, CO and O₂ in the exhaust gas versus mixture equivalence ratio of the triple flame when $V_{in} = 7.0 \text{ m s}^{-1}$.

ratio for the pelton-like flame and traveling flame (see figure 8). The combustion efficiencies for the cases of $\phi = 0.65$ and 1.30 were $\sim 72.4\%$ and $\sim 67.4\%$, respectively (see figure 9).

Figures 10 and 11 show the dependences of the emissions and combustion efficiency, respectively, on the inlet mixture velocity for stoichiometric mixtures. From figure 10, it can be seen that in the inlet mixture velocity range of $1.5\text{--}6.0 \text{ m s}^{-1}$, no unburned CH₄ was detected and the CO concentrations were extremely low. The existences of O₂ concentrations in the exhaust gases are expected to be partly due to the effect of dissociation of combustion products [22]. The stoichiometric fuel–air mixture achieved a combustion efficiency of $\sim 99.6\%$ – 99.7% for the stable circular flame, which can be clearly seen in figure 11. From this figure, it can also be noted that a high combustion efficiency can be maintained over the inlet mixture velocity range of $1.5\text{--}6.0 \text{ m s}^{-1}$ for the stable circular flame. However, when $V_{in} = 6.5 \text{ m s}^{-1}$, which correspond to the unstable circular flame, unburned CH₄ was detected and the concentration of CO also slightly increased, which led to an increase in the O₂ concentration and a decrease in the CO₂ concentration in the exhaust gas (see figure 10). As a

result, the combustion efficiency also decreased to $\sim 95.1\%$ for the unstable circular flame (see figure 11). When $V_{in} = 7.0 \text{ m s}^{-1}$, which correspond to the triple flame pattern, the mole fraction of unburned CH₄ increased significantly and the CO concentration also slightly increased. Meanwhile, a sharp increase in the O₂ concentration and an obvious drop in the CO₂ concentration were observed in the exhaust gas, respectively. Consequently, the combustion efficiency for this case dropped to $\sim 78.8\%$.

Figures 12 and 13 present comparisons between the major combustion products and combustion efficiency for single and double pelton-like flames when $\phi = 0.65$. Although figure 12 has been reported elsewhere [23], we present it here for comparison and discussion. From figure 12, it can be seen that mole fractions of CO₂ and CO for the double pelton-like flame were higher than those of the single pelton-like flame at the same inlet mixture velocity. Meanwhile, the mole fraction of the unburned CH₄ in the exhaust gas of the double pelton-like flame was lower than that of the corresponding single pelton-like flame. Consequently, the combustion efficiency of the double pelton-like flame was higher than that of the

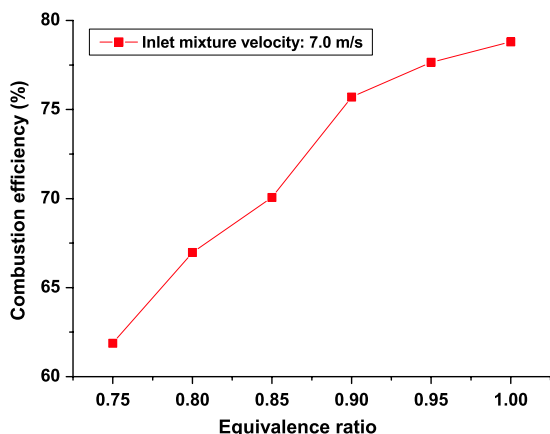


Figure 15. Combustion efficiency versus mixture equivalence ratio of the triple flame when $V_{in} = 7.0 \text{ m s}^{-1}$.

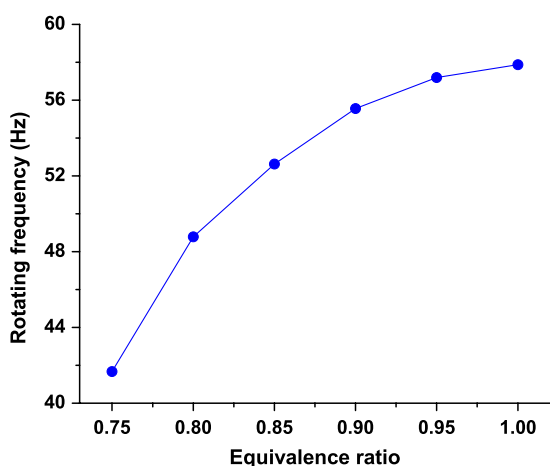


Figure 16. Rotating frequency of the triple flame versus mixture equivalence ratio when $V_{in} = 7.0 \text{ m s}^{-1}$.

single pelton-like flame at the same inlet mixture velocity (see figure 13). These phenomena are thought to be caused by the differences in flame front numbers between the single and double pelton-like flames. For the double pelton-like flame, more fuel was consumed in the combustion process. Those differences were especially obvious when the inlet mixture velocity was increased from 4.5 m s^{-1} to 5.0 m s^{-1} . This is because when the inlet mixture velocity was 5.0 m s^{-1} , the outer tip of the single pelton-like flame almost reached the edges of the circular plates. This indicates insufficient residence time for complete reactions, which led to a high level of unburned fuel leakage and a sharp drop in the combustion efficiency of the single pelton-like flame.

As mentioned in the above, the triple flames were observed at $V_{in} = 7.0 \text{ m s}^{-1}$ over the equivalence ratio range of 0.75–1.0. The influence of the mixture equivalence ratio on the major combustion products for the triple flame is shown in figure 14. From this figure, it can be seen that the unburned CH_4 of the triple flame was very high for all the cases. Moreover, the mole fractions of CO_2 and CO increased with an increasing mixture equivalence ratio, while the mole fractions of O_2 and CH_4 decreased with an increase in the mixture equivalence ratio. These demonstrate that with an increase of

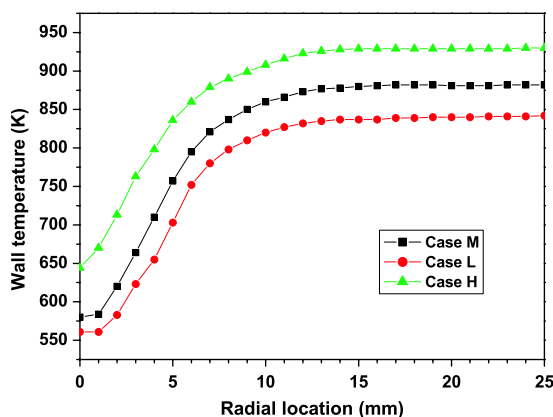


Figure 17. Different wall temperature profiles of the bottom plate created by different heating rates of the burner. The airflow velocities at the delivery tube were 1.0 m s^{-1} .

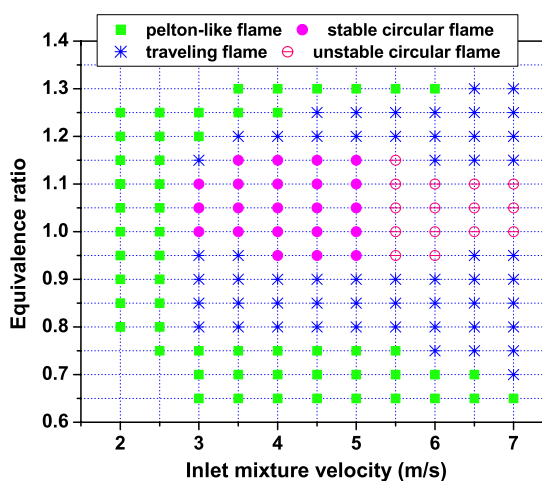


Figure 18. Regime diagram of flame patterns for ‘Case L’.

the mixture equivalence ratio in the fuel-lean side, the local flame propagation velocity also increased. From figure 15, it can be seen that the combustion efficiency of the triple flame increased from $\sim 61.9\%$ to $\sim 78.8\%$ as the mixture equivalence ratio increased from 0.75 to 1.0. Figure 16 shows the rotating frequency of the triple flame versus the equivalence ratio. From this figure, it is noted that the rotating frequency of the triple flame increased with the increase in the mixture equivalence ratio. This indicates that the rotating frequency of the triple flame has a positive correlation with both the local flame propagation velocity and the combustion efficiency.

3.4. Effect of the heat recirculation on combustion stability

The performance of a micro-combustor is strongly influenced by the condition of heat recirculation within the combustor structure [15, 16]. In the present study, the heat recirculation effect of the microchannel is tried to be characterized by different wall temperature levels and their profiles. In order to investigate the effect of these factors on the combustion stability in this configuration, three kinds of wall temperature profiles (including the original one of the foregoing sections) were formed by changing the mass flow rate of the heating

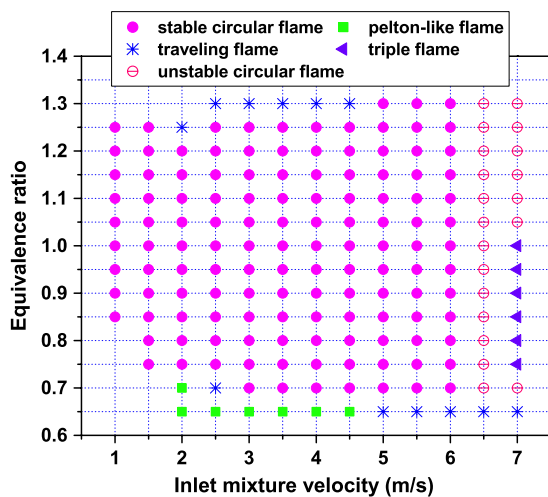


Figure 19. Regime diagram of flame patterns for 'Case H'.

burner. The bottom wall temperature profiles at $V_{in} = 1.0 \text{ m s}^{-1}$ are shown in figure 17, with maximum values to be $\sim 842 \text{ K}$, 882 K and 930 K , respectively. For the convenience of discussion, these three cases are hereafter termed 'Case L', 'Case M' (the original case) and 'Case H', respectively (see figure 17).

Wall temperature level affects the heat exchange between the fuel–air mixture and the walls, and thus changes the reaction rate and the flame speed. As a result, the wall temperature level can impose an effect on pattern formation and stability of the flame, which will affect the combustion completeness and efficiency. However, for simplicity, only the regime diagrams of flame patterns for 'Case L' and 'Case H' are given in figures 18 and 19, respectively, and the comparisons between the combustion products and efficiency at different wall temperature levels are not presented here.

From figure 18, it is noted that the region occupied by the stable circular flame pattern is much narrower than that of figure 5. The stable flame only exists in the inlet mixture velocity range of $3.0\text{--}5.0 \text{ m s}^{-1}$. Most of the regime diagram is dominated by various unstable flame patterns, such as the unstable circular flame, traveling flame and single and double pelton-like flames. Moreover, the flame was not observed at $V_{in} = 1.5 \text{ m s}^{-1}$. All these demonstrate that it was difficult to sustain a stable combustion in this microchannel for 'Case L'.

From figure 19, it can be seen that the region occupied by the stable circular flame pattern becomes much larger than that of figure 5, accompanied by a decrease in the regions occupied by the traveling and pelton-like flames. Moreover, the flame can even be stabilized at the inlet port of the microchannel at $V_{in} = 1.0 \text{ m s}^{-1}$. This demonstrates that the combustion stability limit was broadened to lower the inlet mixture velocity for 'Case H'. However, the flame instability showed little improvement in the high inlet mixture velocity region.

3.5. Recommendations for stable operations

In addition to a stable circular flame, a variety of unstable flame patterns were observed in the radial microchannel. Regime diagrams of flame patterns show that stable and unstable flames are functions of the mixture equivalence ratio, inlet mixture

velocity and heat recirculation condition. Due to a large amount of heat losses, a good heat recirculation is vital to achieve a stable combustion in microscale combustors, while insufficient heat recirculation may reduce the stability limits of these devices. Under a good heat recirculation scenario, the flame can be stabilized in the radial microchannel over wide operating conditions and combustion efficiency does not change much with the inlet mixture velocity and the flame radius for fuel–air mixtures of the same equivalence ratio. This gives us some guidance in the design of micro-combustors with heat recirculation. For example, the performance of the radial micro-combustor can be improved if one selects a wall material with appropriate thermal conductivity to encourage the heat recirculation effect and, meanwhile, decreases the thermal emissivity of the top wall to reduce the heat losses to the ambient surroundings.

The exhaust gas analysis showed that concentrations of unburned CH_4 and CO were much higher for unstable flame patterns than those for a stable circular flame pattern. For stoichiometric and lean mixtures, the stable circular flame can achieve a nearly complete combustion even at low or high inlet velocity (e.g. $V_{in} = 1.5 \text{ m s}^{-1}$ or 6.0 m s^{-1}). The combustion efficiency of the stable circular flames was found to be $\sim 99.6\%$ – 99.9% with the maximum value to be achieved at an equivalence ratio of 0.80. Meanwhile, it is noteworthy that relatively high CO concentration was detected in the exhaust gas of the stable circular flame for fuel-rich mixtures, which led to a decrease in the combustion efficiency. Therefore, a slightly lean mixture (e.g. $\phi = 0.80\text{--}0.95$) is suggested to be used for the radial micro-combustor. A very lean mixture should not be used due to a large amount of unburned fuel leakage, resulting from the existence of various unstable flame patterns. Moreover, it also seems not suitable to use a very high inlet mixture velocity (mass flow rate) due to the existence of unstable flame patterns (e.g., unstable circular flame and triple flame), and even under a good heat recirculation condition these unstable flames cannot be stabilized.

4. Conclusions

Combustion behaviors, such as pattern formations, flame radius, exhaust gas characteristics and heat recirculation effect, have been investigated experimentally in this study. The experimental results showed that flame pattern formation has a critical effect on combustion completeness. A relatively complete combustion and a high efficiency can be achieved when the flame is stable, while in the cases of unstable flame patterns, unburned fuel was found in the combustion products which led to significant reduction in combustion efficiency. In summary, the present work not only can enrich the knowledge of combustion characteristics in radial microchannels, but also may provide some important information for the practical applications of microscale combustion.

Acknowledgment

The authors would like to thank Mr S Hasegawa for helping to conduct the present experiments.

References

- [1] Fernandez-Pello A C 2002 Micro-power generation using combustion: issues and approaches *Proc. Combust. Inst.* **29** 883–99
- [2] Vican J, Gajdeczko B F, Dryer F L, Milius F L, Aksay A and Yetter R A 2002 Development of a micro reactor as a thermal source for MEMS power generation *Proc. Combust. Inst.* **29** 909–16
- [3] Kim N I, Kato S, Kataoka T, Yokomori T, Maruyama S, Fujimori T and Maruta K 2005 Flame stabilization and emission of small Swiss-roll combustors as heaters *Combust. Flame* **141** 229–40
- [4] Pattekar A V and Kothare M V 2004 A micro reactor for hydrogen production in micro fuel cell applications *J. Microelectromech. Syst.* **13** 7–18
- [5] Epstein A H, Senturia S D and Anthasuresh G 1997 Power MEMS and microengines *IEEE Transducers '97 Conf. (Chicago, IL)* pp 753–6
- [6] Mehra A, Zhang X, Ayon A A, Waitz I A, Schmidt M A and Spadaccini C M 2000 A six-wafer combustion system for a silicon micro gas turbine engine *J. Microelectromech. Syst.* **9** 517–27
- [7] Spadaccini C M, Mehra A, Lee J, Zhang X, Lukachko and Waitz I A 2003 High power density silicon combustion system for micro gas turbine engines *J. Eng. Gas Turbines Power* **125** 709–19
- [8] Hua J, Wu M and Kumar K 2005 Numerical simulations of the combustion of hydrogen air mixture in micro-scaled chambers: II. CFD analysis for a micro combustor *Chem. Eng. Sci.* **60** 3507–15
- [9] Wu M, Hua J and Kumar K 2005 An improved micro combustor design for micro gas turbine engine and numerical analysis *J. Micromech. Microeng.* **15** 1817–23
- [10] Dumand C, Guidez J, Orain M and Sabel'nikov V A 2005 Specific problems of micro-turbine for micro-drones application *Eur. Conf. for Aerospace Sciences (Moscow)*
- [11] Verstraete D and Trilla J 2006 Development of a combustion chamber for an ultra micro gas turbine *7th National Conf. on Theoretical and Applied Mechanics (Mons, Belgium)*
- [12] Yuasa K, Oshimi K, Nose H and Tennichi Y 2005 Concept and combustion characteristics of ultra-micro combustors with premixed flame *Proc. Combust. Inst.* **30** 2455–62
- [13] Yang W M, Chou S K, Shu C, Li Z W and Xue H 2007 Experimental study of micro thermophotovoltaic systems with different combustor configurations *Energy Convers. Manage.* **48** 1238–44
- [14] Lloyd S A and Weinberg F J 1974 A burner for mixtures of very low heat content *Nature* **251** 47–8
- [15] Ronney P D 2003 Analysis of non-adiabatic heat recirculating combustors *Combust. Flame* **135** 421–39
- [16] Norton D G and Vlachos D G 2003 Combustion characteristics and flame stability at the microscale: a CFD study of premixed methane/air mixtures *Chem. Eng. Sci.* **58** 4871–82
- [17] Maruta K, Kataoka T, Kim N I, Minaev S and Fursenko R 2005 Characteristics of combustion in a narrow channel with a temperature gradient *Proc. Combust. Inst.* **30** 2429–36
- [18] Kumar S, Maruta K and Minaev S 2007 Experimental investigations on the combustion behavior of methane-air mixtures in a microscale radial combustor configuration *J. Micromech. Microeng.* **17** 900–8
- [19] Kumar S, Maruta K and Minaev S 2007 Pattern formation of flames in radial microchannels with lean methane-air mixtures *Phys. Rev. E* **75** 016208
- [20] Kumar S, Maruta K and Minaev S 2007 On the formation of multiple rotating platen-like flame structures in radial microchannels with lean methane-air mixtures *Proc. Combust. Inst.* **31** 3261–8
- [21] Jackson T L, Buckmaster J, Lu Z, Kyritsis D C and Massa L 2007 Flames in narrow circular tubes *Proc. Combust. Inst.* **31** 955–62
- [22] Turns S R 2000 *An Introduction to Combustion* 2nd edn (New York: McGraw-Hill)
- [23] Fan A W, Minaev S, Kumar S, Liu W and Maruta K 2007 Regime diagrams and characteristics of flame patterns in radial microchannels with temperature gradients *Combust. Flame* submitted